

Large Language Models Encode Semantics in Low-Dimensional Linear Subspaces

Baturay Saglam^{1,2}, Paul Kassianik², Blaine Nelson²
 Sajana Weerawardhena², Yaron Singer², Amin Karbasi²

¹Yale University
²Foundation AI – Cisco Systems Inc.

Abstract

Understanding the latent space geometry of large language models (LLMs) is key to interpreting their behavior and improving alignment. However, it remains unclear to what extent LLMs internally organize representations related to semantic understanding. To investigate this, we conduct a large-scale empirical study of hidden states in transformer-based LLMs, analyzing 11 decoder-only models across 6 scientific topics and 12 layers each. We find that high-level semantic information consistently lies in low-dimensional subspaces that form linearly separable representations across distinct domains. This separability becomes more pronounced in deeper layers and under prompts that trigger structured reasoning or alignment behaviors—even when surface content is unchanged. This geometry enables simple yet effective causal interventions in hidden space; for example, reasoning patterns like chain-of-thought can be captured by a single vector direction. Together, these findings support the development of geometry-aware tools that operate directly on latent representations to detect and mitigate harmful or adversarial content, using methods such as transport-based defenses that leverage this separability. As a proof of concept, we demonstrate this potential by training a simple MLP classifier as a lightweight latent-space guardrail, which detects adversarial and malicious prompts with high precision.

1 Introduction

Large language models (LLMs), trained on vast textual corpora for next-token prediction, have become versatile systems capable of generating coherent and contextually relevant text across a wide range of semantic domains. Their proficiency ranges from shallow semantic understanding (e.g., basic word sense disambiguation) to engaging in structured reasoning and ethical deliberation. Despite these impressive capabilities, our understanding of how these models internally organize and encode such diverse semantic knowledge remains incomplete. A crucial step toward enhanced interpretability and safer deployment involves investigating how semantic distinctions manifest within the hidden representations of models.

Recent interpretability studies suggest that neural networks, including transformer-based LLMs, encode semantic and behavioral attributes within structured, often linear subspaces of their latent representations [35, 33]. Known as the *linear representation hypothesis* (LRH), this perspective has motivated research showing that high-level concepts—ranging from linguistic structure to sentiment—can frequently be captured or manipulated by simple linear operations on hidden states [7, 14]. Although these findings suggest promising geometric structure, they have typically focused on highly specific lexical features (e.g., whether a sentence mentions a “cat”) [16], narrow domains

(e.g., word embeddings) [20], or contrasting genres of text (e.g., symbolic versus natural language) [28]. There remains a broader question of to what extent linearly structured representations exist across diverse, high-level semantic content in a model-agnostic manner.

In this paper, we conduct a large-scale empirical study of latent space representations across diverse model configurations and semantic domains. We analyze hidden representations from **11 decoder-only, transformer-based LLMs** of varying sizes, spanning **12 layers per model** and **6 high-level scientific topics**. Our experiments uncover several core trends:

- (i) **Models compress semantics into low-dimensional linear subspaces.** We show that high-level semantic understanding (e.g., math, physics, biology) is encoded in low-dimensional linear subspaces of hidden space (Section 5.1). As a complementary result, we find that this compression does not necessarily concentrate at a particular layer depth, in contrast to what prior work has suggested [4, 41, 47, 38].
- (ii) **High-level semantics are represented by linearly separable clusters.** Within the range of domains and prompts we study, representations of text with different semantic content exhibit a linearly separable clustering pattern (Section 5.2). This separability increases toward the final layers, as indicated by rising linear classification accuracy—eventually leading to more semantically distinct domains becoming linearly separable.
- (iii) **Instructions sharpen and disentangle latent representations.** Prompts that instruct structured reasoning—such as chain-of-thought—or that trigger alignment behavior, lead to distinct and linearly separable internal representations, revealing how user instructions and requests shape model responses (Sections 6.1, 6.2).

These findings suggest that both high-level semantics and alignment-relevant behaviors are encoded in structurally coherent and linearly accessible ways within the hidden spaces of LLMs. This representational geometry enables practical interventions—such as linear classifiers or transport-based defenses—that can detect, characterize, or suppress adversarial or harmful content by acting directly on internal representations. To demonstrate this, we build a lightweight latent-space guardrail using a simple multi-layer perceptron to defend against adversarial and harmful prompts (Section 6.2.2). This guardrail offers effective protection with minimal overhead. We see our this as a promising direction for interpretability, alignment, and safety, and release our code to support further research in this area.¹

2 Related Work

2.1 Intrinsic Dimensionality of Representations

Early studies on contextual embeddings found that transformer representations occupy low-dimensional manifolds relative to their full representational capacity [1, 18, 19, 11]. These findings are typically supported by PCA or SVD analyses, which reveal steep spectral decay in hidden layers. Later work attributed lower intrinsic dimensionality to factors such as token frequency, residual connections, or architecture-specific effects [20, 38].

While consistent with our observation that LLMs compress semantic information, prior studies focus mainly on word embeddings [20] or bidirectional architectures. In contrast, we analyze the intrinsic dimensionality of hidden states across high-level semantic categories and recent autoregressive models—including Mistral, Llama 3, and the Gemma series.

¹<https://github.com/baturaysaglam/llm-subspaces>

2.2 Semantic Probing and Linearity in Representations

Several studies have shown that linguistic features—such as part-of-speech, dependency relations, or sentiment (e.g., “is an equation”)—can be recovered via linear probes applied to hidden states [14, 29, 46]. Structural probes have revealed low-rank subspaces corresponding to syntax trees [24], while other work has identified interpretable directions encoding higher-level concepts such as truthfulness [6, 5, 31, 34], formality [10], and periodic patterns like days of the week [17]. Concept vectors derived from these directions—using nonlinear techniques like kernel methods or sparse autoencoders—have also been used to steer model outputs at inference time [17, 6, 15]. Separability has likewise been observed between arithmetic expressions (e.g., $2 + 1 = 3$) and general language representations [28]. This extends insights from neuroscience-inspired studies [30, 22], which analyze transformer circuits [16].

Our work differs in several key ways. First, we study the linearity in broader, higher-order semantics—topics like electrical engineering or statistics—that are *more composite* than isolated attributes and span thousands of those fine-grained features examined in prior work. Second, we show that these topics are captured along a few dominant directions in the hidden space, forming low-rank linear subspaces that extend earlier findings to more abstract and broader domains. Third, while prior studies often rely on nonlinear methods, we find that linear separability emerges naturally for high-level semantic distinctions—suggesting a *simpler* and *more structured* internal geometry. Lastly, our approach is fully unsupervised and model-agnostic, relying solely on unmodified hidden states—a commonly studied, fundamental form of internal representation—offering a minimally intrusive and comprehensive view of how semantic structure arises in LLMs.

3 Background

We outline the technical preliminaries and analytical tools that underpin our experiments.

3.1 Transformer Architecture and Hidden Representations

Transformer-based [48] language models operate through a sequence of layers that apply multi-head self-attention followed by feedforward transformations. Given a token sequence, each layer computes a hidden representation $\mathbf{h} \in \mathbb{R}^d$ for each token, where d denotes the hidden dimensionality. The model is composed of L such hidden layers, stacked sequentially to progressively refine the token representations.

In multi-head self-attention, the hidden state \mathbf{h} is linearly projected into query, key, and value matrices: $\mathbf{Q}_i = \mathbf{h}W_i^Q$, $\mathbf{K}_i = \mathbf{h}W_i^K$, and $\mathbf{V}_i = \mathbf{h}W_i^V$ for each head $i = 1, \dots, H$, where $W_i^Q, W_i^K, W_i^V \in \mathbb{R}^{d \times d_H}$ are learned parameters. Each head computes attention as:

$$\text{head}_i = \text{softmax} \left(\frac{\mathbf{Q}_i \mathbf{K}_i^\top}{\sqrt{d_H}} \right) \mathbf{V}_i.$$

where $d_H = d/H$. The outputs of all heads are concatenated and projected to form the next hidden state:

$$\text{MultiHead}(\mathbf{h}) = \text{Concat}(\text{head}_1, \dots, \text{head}_H)W^O,$$

where $W^O \in \mathbb{R}^{d \times d}$ is a learned output projection matrix. This structure allows each head to capture distinct relational patterns across tokens in different subspaces of the hidden representation.

3.2 Subspace Analysis via SVD

To analyze the d -dimensional subspace spanned by N observations, we examine the row space of the data matrix $\mathbf{X} \in \mathbb{R}^{N \times d}$. Each row of \mathbf{X} represents a sample in \mathbb{R}^d , so the row space captures the directions of variation in the data. Singular value decomposition (SVD) provides an orthonormal basis for both the row and column spaces of \mathbf{X} . Specifically, decomposing \mathbf{X} as

$$\mathbf{X} = \mathbf{U}\Sigma\mathbf{V}^\top$$

yields $\mathbf{V}_{\text{SVD}} \in \mathbb{R}^{d \times d}$, where the columns of \mathbf{V}_{SVD} are the right singular vectors. We use the subscript “SVD” to avoid confusion with the value matrix in attention. These vectors span the row space of \mathbf{X} and are ordered by their corresponding singular values in Σ , which reflect the variance captured along each direction.

Basis Vectors from \mathbf{V}_{SVD} The columns of \mathbf{V}_{SVD} form an orthonormal basis for the row space and serve as the *principal components* (PCs), ordered by decreasing variance. The number of strictly positive singular values indicates the number of orthogonal directions spanned by the data, or the *rank of \mathbf{X}* , which is at most $\min(N, d)$. Selecting the first r columns of \mathbf{V}_{SVD} , where r is this rank, yields a compact and meaningful representation of the data subspace.

3.3 Linear Separability

A simple and fast way to assess the linear separability of two data clusters is by fitting a linear classifier. We use a hard-margin support vector machine (SVM) to find a separating hyperplane. For a dataset of N samples (\mathbf{x}_i, y_i) , where $\mathbf{x}_i \in \mathbb{R}^d$ is a feature vector and $y_i \in \{-1, 1\}$ is the corresponding class label (representing two different topics in our case), the SVM solves the constrained optimization problem:

$$\begin{aligned} \min_{\mathbf{w}, b, \xi} \quad & \frac{1}{2} \|\mathbf{w}\|^2 + C \cdot \mathbf{1}^\top \xi \\ \text{s.t.} \quad & y_i(\mathbf{w}^\top \mathbf{x}_i + b) \geq 1 - \xi_i \quad \forall i = 1, \dots, N \\ & \xi_i \geq 0 \end{aligned} \tag{1}$$

where $\mathbf{w} \in \mathbb{R}^d$ and $b \in \mathbb{R}$ define the separating hyperplane ($\mathbf{w}^\top \mathbf{x} + b = 0$). The term $\frac{1}{2} \|\mathbf{w}\|^2$ regularizes the margin, while the slack variables ξ_i capture classification errors. The regularization parameter $C > 0$ controls the trade-off between maximizing the margin and minimizing classification errors. A large C imposes a high penalty on errors, pushing the model to separate the data more strictly, often resulting in a narrower margin.

To test for linear separability, we approximate a hard-margin setting by setting $C = 10^{10}$ and a small optimization tolerance ($\text{tol} = 10^{-12}$). With this setup, any non-zero ξ_i is heavily penalized, and the optimizer seeks a solution where all $\xi_i \approx 0$. If the resulting classifier achieves perfect accuracy (i.e., zero classification error), we conclude that a separating hyperplane exists and label the cluster pair as *linearly* separable. For efficient testing, we use the CUDA-accelerated SVM from the cuML library [37], rather than solving for arbitrary hyperplanes without margin regularization; see Appendix A.2 for details.

4 Experimental Design

Further details of our experimental setup are provided in Appendix A.

4.1 Models

We assembled a diverse set of decoder-only autoregressive transformers spanning a range of configurations and developers. To study scaling effects and intra-family consistency, we included multiple size variants from the same model series. All models are open-source, and the details are summarized in Table 1.

Model	Size	Model Dim. d	# Layers	Developer	Release Date
Mistral Small 3 (2501) [2]	24B	5120	40	Mistral AI	Jan. 2025
Mistral [25]	7B	4096	32	Mistral AI	Sep. 2023
Llama 3.1 [3]	8B	4096	32	Meta	Jul. 2024
Llama 3.2 [3]	3B	3072	28	Meta	Jul. 2024
Gemma 2 [45]	9B	3584	42	Google	Jun. 2024
Gemma 2 [45]	2B	2304	26	Google	Jul. 2024
GPT-J [42]	6B	4096	28	Eleuther AI	Jun. 2021
GPT-2 XL [36]	1.5B	1600	48	OpenAI	Nov. 2019
GPT-2 Large [36]	774M	1280	36	OpenAI	Aug. 2019
GPT-2 Medium [36]	355M	1024	24	OpenAI	May 2019
GPT-2 [36]	124M	768	12	OpenAI	Feb. 2019

Table 1: Open-source decoder-only autoregressive models selected for empirical studies.

4.2 Dataset

arXiv Abstracts We reviewed over 100 datasets on Hugging Face and Kaggle and selected the arXiv metadata dataset [12] for its rich coverage and structured format. The dataset contains titles, authors, and abstracts of arXiv articles from the past 30 years, categorized according to the arXiv taxonomy². Using abstracts ensures consistent length and structure (e.g., an introductory sentence followed by a problem description) while also guaranteeing that the content is human-written, avoiding distributional bias from LLM-generated text. The covered STEM fields include computer science (CS), economics, electrical engineering and systems science (EESS), mathematics, physics, quantitative biology, quantitative finance, and statistics.

Preprocessing We did not modify any samples beyond basic string cleanup, such as stripping whitespaces. To ensure clear categorical distinction, we removed samples associated with multiple meta taxonomies and discarded abstracts with fewer than 20 tokens to ensure sufficient semantic content for model processing. After preprocessing, the economics and quantitative finance categories contained fewer than 4,000 samples—less than the hidden dimensionality of some models. In such cases, all sets are trivially linearly separable. As a result, we excluded these categories. Token counts per sample range from 20 to roughly 1,000. To manage computational costs, we capped each sample at 750 tokens and limited each dataset to a maximum of 20,000 samples. Token and sample statistics for each topic are provided in Appendix A.1.

²https://arxiv.org/category_taxonomy

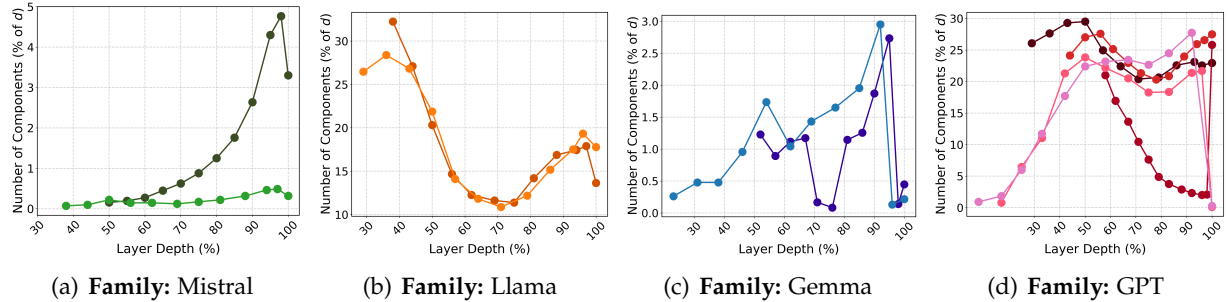


Figure 1: Percentage of principal components (relative to hidden dimensionality) required to explain at least 90% of the total variance in *physics* abstracts, plotted across layer depth. **Darker colors** indicate the larger model within each family.

4.3 Extracting Model Hidden States

We passed each topic dataset through the models and collected hidden states at several layers immediately before the generation of the first token. To ensure a depth-aware and representative analysis, we extracted hidden states from the last 12 layers at every second layer, including the penultimate and final layers. As a result of this collection process, we obtain a data matrix for each topic t_i per model, denoted as $\mathbf{X}^{(t_i)} \in \mathbb{R}^{N_{t_i} \times d}$, where N_{t_i} is the number of samples in the dataset of topic t_i . Hence, each row $\mathbf{X}_i^{(t_i)}$ is a d -dimensional vector in \mathbb{R}^d for $i = 1, \dots, N_{t_i}$.

5 Findings on Effective Dimensionality and Linear Separability

We evaluate hidden states from 6 arXiv meta categories across 11 models, totaling 128 layers (12 per model, 8 for GPT-2). Due to the large volume of results, we present representative subsets that capture core patterns and key exceptions. Full results are available on our GitHub¹. We also exclude low-dimensional visualizations, as standard techniques often distort high-dimensional geometry.

5.1 Effective Dimensionality

Figure 1 depicts the number of components to explain the 90% of the variance in text dataset.

High-level semantics reside in low-dimensional subspaces of \mathbb{R}^d . Across all models, a small number of principal components—often under 10% of the total dimensionality—account for nearly all the variance in hidden states. While the clusters formally span \mathbb{R}^d (i.e., all singular values are positive), their effective dimensionality is much lower. This indicates that high-level semantic understanding concentrate in compact—and thus approximately linear—subspaces, meaning they lie near a low-dimensional affine subspace of \mathbb{R}^d .

Importantly, the remaining singular values, though small, are not necessarily redundant. The leading principal components capture dominant structure—e.g., that a passage is broadly about physics—while lower-variance components may encode finer-grained content, such as references to fluid dynamics or condensed matter. This extends the superposition hypothesis [16] and supports the findings of Engels et al. [17], suggesting that a few interpretable features (i.e., the leading PCs) may suffice to represent the broader semantic category within the model.

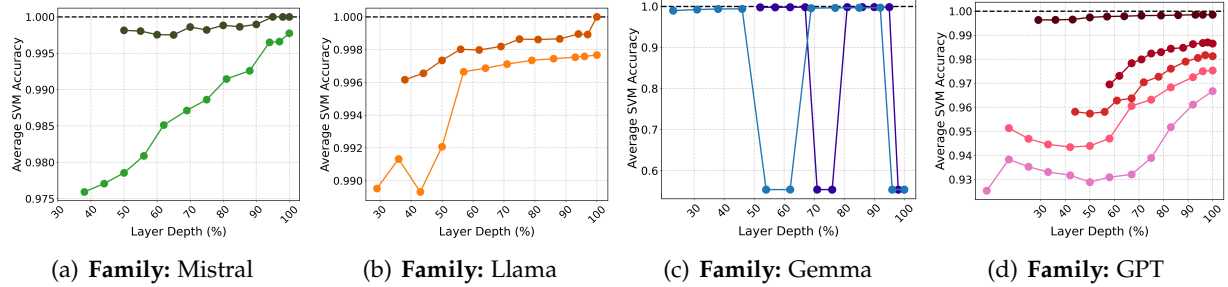


Figure 2: SVM classification accuracy averaged over all 15 topic pairs as a function of layer depth. **Darker colors** indicate the larger model within each family. The sub-1.0 average accuracy reflects that while some topic pairs are not linearly separable, they still achieve high accuracy.

Lastly, prior work has observed U-shaped (or bell-shaped) curves in information density across layers, indicating that text information is most compressed in the intermediate layers of neural networks [4] and transformers [41, 47, 38]. As a side result, our findings show that this trend does not necessarily hold for high-level semantics and varies by model. For example, Mistral-24B, Gemma-2B, and GPT-2 exhibit peak compression in early layers, while the Llama models follows the previously observed pattern. These differences highlight the need for further studies to better understand how information is distributed across architectures.

5.2 Linear Separability

Figure 2 reports SVM accuracy averaged over all 15 topic pairs (six topics, with unordered pairwise combinations) as a function of model depth. Table 2 details the separability in the most linearly separable layer of each model.

Semantic separability emerges and sharpens in final layers. Although the scientific topics are closely related (e.g., math appears across multiple fields), the representations of the meta categories are largely linearly separable. Within each model family, increasing the parameter count—and thus the hidden dimensionality—consistently improves separability, as higher-dimensional spaces are better suited to capture and disentangle complex semantic structure. The slightly below-1.0 average SVM accuracy indicates that some topic pairs are not perfectly separable, lowering the overall average from perfect linear separation. Table 2 highlights the number of fully separable topic pairs..

Furthermore, such disentanglement becomes increasingly pronounced toward the final layers, except for Gemma models (see the subsequent discussion). This trend aligns with the decoder’s objective in next-token prediction, where the final hidden states must support a linear projection onto vocabulary logits. By the top layers, models rotate and refine representations such that semantic subspaces—like topic—become linear and nearly orthogonal, enabling simple dot products to favor the correct tokens.

Self-attention appears to structure hidden geometry. Unlike earlier findings in RNNs—where semantic representations were often only *partially* or *locally* separable [32]—we observe clear and consistent clustering in transformers. This stronger structure likely stems from the self-attention mechanism, which enables dynamic routing of contextual information and supports the formation

of well-separated topic clusters, as suggested by prior work showing the role of attention heads in semantic encoding (e.g., in safety) [51].

In line with this, self-attention may explain the distinct sawtooth-like pattern observed in Gemma models. This behavior likely stems from Gemma’s unique architecture—the interleaved attention mechanism—which alternates between global attention layers that capture document-level semantics and local attention layers with limited context window. The resulting high- and low-separability layers may correspond to these alternating global and local mechanisms. However, further investigation is needed to fully understand this exception.

Model	Most Separable Layer	Linearly Separable Pairs	Non-Separable Pairs
Mistral-24B	38, 39, 40 (100%)	15/15	-
Mistral-7B	32 (99.77%)	14/15	CS-EESS
Llama 3.1-8B	32 (100%)	15/15	-
Llama 3.2-3B	28 (99.77%)	14/15	CS-EESS
Gemma 2-9B	40 (99.84%)	14/15	CS-EESS
Gemma 2-2B	24 (99.70%)	13/15	CS-EESS, CS-Stat
GPT-J (6B)	28 (99.851%)	14/15	CS-EESS
GPT-2 XL (1.5B)	47 (98.70%)	8/15	CS-EESS, CS-Stat, Physics-Math...
GPT-2 Large (774M)	35 (98.17%)	5/15	CS-EESS, CS-Stat, Physics-Math...
GPT-2 Medium (355M)	24 (97.53%)	0/15	All
GPT-2 (124M)	12 (96.68%)	0/15	All

Table 2: Linear separability results in the most separable layer of each model, as measured by average SVM accuracy across topic pairs (shown in parentheses). We report the number of linearly separable topic pairs and list the specific pairs that are not separable. For brevity, long lists of non-separable cases are not fully listed. As model scale decreases, closely related fields—such as CS-EESS (e.g., systems and control) and CS-Statistics (e.g., machine learning)—begin to show entangled representations.

5.3 Impact of Domain-Specific Keywords on Separability

The presence of domain-specific keywords can significantly affect the structure of representations, including their linear separability. To study this, we mask topic-specific keywords in abstracts in a controlled manner and evaluate SVM accuracy on the resulting representations.

However, manually identifying keywords across all subtopics within each meta category would be exhaustive. Instead, we assume that domain-specific keywords are typically rare and have low frequency in the English language. To approximate this, we use the English Word Frequency dataset [44], which contains 333,333 single words along with their frequency ranks. Given a text and a frequency threshold (ranging from 0–99%), we mask words that fall below the threshold using a special mask token, based on their frequency. Specifically, words are grouped into buckets according to their log frequency, which guides the masking process. As the threshold increases, more frequent keywords are masked.

Figure 3 presents our sensitivity analysis. Linear separability is lost after masking just 10% of the most frequent keywords for the CS-EESS pair, indicating a particularly fragile boundary between these closely related domains—likely due to substantial lexical overlap and shared conceptual foundations. In contrast, the persistence of high accuracy up to the 50–60% threshold in other pairs suggests that domain-specific information is not concentrated in a small set of keywords but is distributed across implicit cues—such as syntactic structure or taxonomical language patterns—that

preserve domain distinctions even under substantial masking. Beyond 60%, the masked text appears generic and could plausibly belong to any broad technical field; see Appendix B.1 for examples at 0%, 10%, and 50% masking.

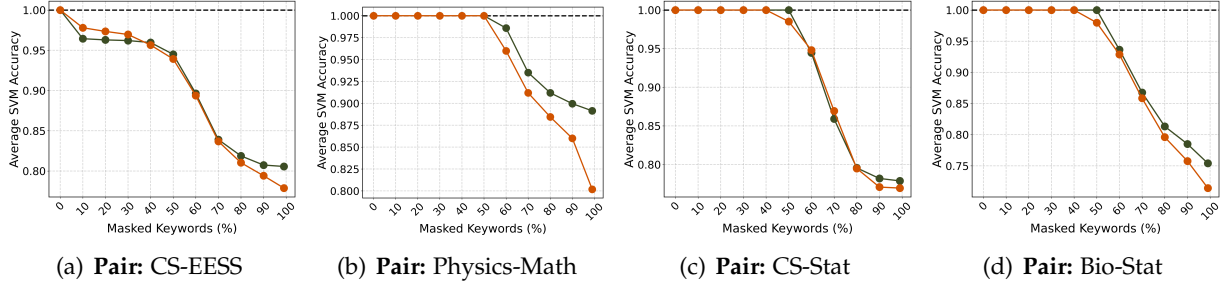


Figure 3: SVM classification accuracy on example pairs of closely related topics as a function of the keyword-masking threshold. Results are shown for Mistral-24B (dark green) and Llama 3.1-8B (dark orange), the two models that exhibit linear separability across all topic pairs.

6 Implications for Reasoning and Alignment

Building on our findings, instruction-tuned (IFT) and aligned models may also organize their representations into linearly separable manifolds based on user instructions and aligned behavior. We investigate whether similar geometry also appears during reasoning—e.g., under chain-of-thought prompting—and when models are prompted with adversarial or harmful content.

6.1 Reasoning

We begin with a simple form of reasoning: assessing whether a *one-sentence* chain-of-thought (CoT) instruction induces geometric changes in the hidden space of IFT models. To test this, we use the questions from the benchmarks: CommonsenseQA [43], GSM8K [13], and MMLU [23]. We present the exact same questions to the models, both with and without the CoT instruction: “Think step by step and show all your reasoning before giving the final answer.” Thus, any representational changes will be solely due to the CoT instruction, which corresponds to ~15 tokens.

Using the same linear separability analysis (and layers) from Section 5.2, we evaluate the IFT variants of Mistral and Llama models. The results are reported in Table 3.

Instructions like CoT sharpen representational disentanglement. Strikingly, linear separability is far more frequent than in topic-based evaluations, despite the CoT and non-CoT inputs differing by just *one instruction sentence* (or an additional 15 tokens). This minor prompt narrows the model’s output space, leading to more consistent completions (e.g., “Let’s analyze each option...”) and tighter clustering in hidden space. In contrast, open-ended prompts (as in topic datasets) yield diverse continuations, dispersing representations across broader semantic regions.

This effect mirrors the findings of Saglam et al. [40], who showed that in-context learning induces task-specific shifts in the distribution of final-layer activations. Similarly, the CoT instruction compresses the output distribution into a distinct, instruction-driven subspace—enabling more structured and interpretable model behavior.

Chain-of-thought can be encoded in a single d -dimensional vector. To further test the linearity of representations, we perform controlled steering experiments using the centroid-difference vector between topic clusters—assessing whether movement along this direction causally and meaningfully alters model outputs. The intervention proves effective: adding the centroid-difference vector to the hidden states at the final token position reliably induces CoT-style responses. This suggests that a single vector in the model’s hidden space can encode CoT reasoning. Details and model outputs are provided in Appendix B.2. While these results offer preliminary causal evidence, a more formal and comprehensive set of intervention studies—such as adversarial perturbation analysis or axis-orthogonality tests—is left for future work, given the breadth of experiments already included.

Model	CommonsenseQA	GSM8K	MMLU
Mistral-24B (IFT)	12/12	12/12	12/12
Mistral-7B (IFT)	12/12	12/12	12/12
Llama 3.1-8B (IFT)	12/12	12/12	11/12
Llama 3.2-3B (IFT)	12/12	12/12	7/12

Table 3: Linear separability analysis of the representations of the same question with and without the chain-of-thought instruction. The number of separable cases is reported. Instruction-following behavior leads to a representational shift that forms a new, linearly separable cluster.

6.2 Alignment

We test whether representations of harmful and benign prompts are linearly separable and how they are structured in hidden space. Using the WildJailbreak dataset [27], we compare two types of query narratives: (i) vanilla and (ii) adversarial. Regardless of framing, each query is either harmful or benign. While vanilla prompts are straightforward, structurally adversarial prompts (e.g., those framed as tricky narrative scenarios) may still be benign in meaning, and well-aligned models should treat them accordingly. In contrast, harmful prompts remain harmful regardless of phrasing. Details about WildJailbreak are provided in Appendix A.1.

Since separability emerges most strongly in final layers, we performed our tests at the final layer of the selected IFT models. Results, consistent across all four chat models, are reported in Table 4. Figure 4 further illustrates the overarching global pattern.

Hidden representations reflect alignment and adversarial vulnerability. A consistent pattern holds across all models: aligned IFT models clearly separate safe and harmful vanilla prompts in the hidden space, and both are well-separated from adversarial ones. This is expected, as these models undergo safety training, and adversarial prompts often use narrative or hypothetical framing that shifts internal representations by altering context and response expectations. Furthermore, models often generate compliant responses to harmful adversarial queries, reflecting the representational overlap between adversarial but benign prompts. This entanglement is natural, as adversarial prompts are explicitly crafted to resemble benign queries and mislead the model.

Model	Benign \leftrightarrow Malicious	Benign \leftrightarrow Adv.	Mal. \leftrightarrow Adv.	Adv. Benign \leftrightarrow Adv. Mal.
Mistral-24B (IFT)	0.86 ✓	1.13 ✓	1.08 ✓	0.80 ✗
Mistral-7B (IFT)	0.78 ✓	2.34 ✓	2.01 ✓	0.61 ✗
Llama 3.1-8B (IFT)	0.61 ✓	1.02 ✓	0.88 ✓	0.40 ✗
Llama 3.2-3B (IFT)	0.35 ✓	0.56 ✓	0.50 ✓	0.23 ✗

Table 4: Wasserstein distances across the clusters of vanilla benign, vanilla malicious (mal.), adversarial benign, and adversarial malicious (adv. mal.) prompts from the WildJailbreak dataset. Vanilla prompts are compared against the unity of the adversarial (both benign and malicious) prompts. Cluster pairs identified as linearly separable are marked with “✓”. Distance values are smoothed using the $\log(1 + x)$ transformation to reduce the impact of scale differences caused by varying hidden dimensionalities.

6.2.1 Why Linear Separability is Important

Linear separability offers promising opportunities for building AI defenses against adversarial attacks and harmful inputs by operating directly in latent space. One immediate application is adversarial prompt classification: when adversarial and non-adversarial inputs are linearly separable, simple classifiers (e.g., hard-margin SVMs) can detect adversarial queries with perfect accuracy. Once detected, hardcoded safeguards can be triggered to neutralize the threat.

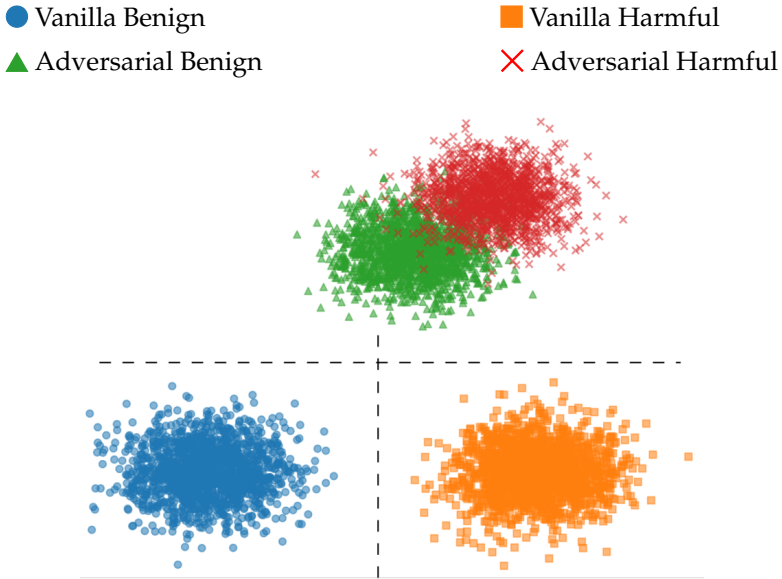


Figure 4: Conceptual illustration of the hidden space structure based on linear separability experiments in Table 4. Distances and cluster sizes reflect Wasserstein distances and cluster variances, respectively. Linear separability is indicated with dashed lines.

In a more automated setting, linear separability implies that adversarial and vanilla clusters have disjoint convex hulls. This makes the projection problem well-posed with strong duality and constrains feasible transport plans to align with the latent geometry. While transport-based methods can be computationally demanding in high-dimensional spaces, they offer a principled basis for intervention. For example, hidden states of adversarial prompts could be “purified” by

True / Pred	Van. Benign	Van. Harmful	Adv. Benign	Adv. Harmful
Van. Benign	1000	0	0	0
Van. Harmful	0	1000	0	0
Adv. Benign	0	1	150	59
Adv. Harmful	1	26	59	1914

Table 5: Confusion matrix of our latent-space guardrail evaluated on the augmented WildJailbreak test set. The classifier is trained on the final hidden layer of the instruct-finetuned Llama 3.1-8B used as the underlying aligned model.

Class	Precision	Recall	F1-Score	Support
Vanilla Benign	1.0	1.0	1.0	1000
Vanilla Harmful	0.97	1.0	0.99	1000
Adversarial Benign	0.72	0.71	0.72	210
Adversarial Harmful	0.97	0.96	0.96	2000

Table 6: Performance metrics of our latent-space guardrail evaluated on the augmented WildJailbreak test set. The classifier operates on the final hidden layer of the instruct-finetuned Llama 3.1-8B used as the underlying aligned model.

generative models that map them to their nearest vanilla counterparts in latent space. Since the distributions are clearly separated (in a finite-sample sense), these models can learn simple, stable mappings between them—reducing complexity and improving training efficiency. We leave the development of such methods to future work.

6.2.2 Defense from Within: A Lightweight Latent-Space Guardrail

As a proof of concept, we train a simple neural network that classifies prompts in latent space to provide a lightweight defense against harmful inputs. We train a 7-layer MLP (2048-2048-1024-1024-512-64 hidden units) to detect the adversarialness and harmfulness of prompts based on their latent representations. This results in a 4-class classification task: adversarial vs. vanilla and benign vs. harmful. We run experiments using the final hidden layer of instruct-finetuned Llama 3.1-8B model as the base aligned model.

We evaluate the model on the WildJailbreak test set, which originally contained 210 adversarial harmful and 2,000 adversarial benign prompts. To balance the dataset, we added 1,000 vanilla benign and 1,000 vanilla harmful prompts not seen during training, bringing the total to 4,120 samples. The corresponding confusion matrix and performance metrics are shown in Figures 5 and 6. We also provide a *cookbook* in our repository¹ that outlines the steps for building this latent-space guardrail.

Results show that our latent-space classifier performs effectively across diverse prompt types. With an overall **accuracy of 96.53%** and a **weighted F1 score of 0.97**, the model reliably classifies prompts even under mixed distributions of benign and harmful inputs, in both vanilla and adversarial forms. The high **AUC of 0.9931** over benign versus harmful prompts (regardless of adversarialness) suggests that the final hidden states may encode a clear, separable notion of harmfulness. Training such a lightweight MLP—completed in minutes and operating entirely in latent space—demonstrates that internal model structure can support an efficient additional defense layer without requiring full decoding or external content analysis.

While the classifier performs reliably on vanilla prompts, its performance on adversarial cases—particularly adversarial benign prompts—is comparatively lower. The **adversarial macro F1 of 83.97%** reflects this gap, indicating that prompts with obfuscated intent or indirect framing are more difficult to classify accurately. In these cases, the model may occasionally overflag benign inputs or underflag subtle harmful ones. Although this limitation does not strictly undermine the overall utility of the latent-space approach, it highlights the need for further work to improve robustness under adversarial conditions. Future efforts may focus on expanding the coverage of such cases through more diverse training examples or combining the latent-space classifier with additional detection layers.

7 Conclusion

We conducted a large-scale empirical study of latent space geometry in decoder-only large language models (LLMs), focusing on the emergence of low-dimensional subspaces and their linear separability with respect to high-level semantic understanding. Analyzing 11 decoder-only models across 6 scientific disciplines and 12 layers each, we found that semantic representations consistently compress into compact regions of the hidden space and form linearly separable clusters. These patterns hold across diverse models and support the view that LLMs organize broad semantic knowledge along interpretable linear dimensions.

Such semantic disentanglement strengthens in deeper layers and is amplified by reasoning prompts, such as chain-of-thought (CoT) or adversarial content, reflecting a layerwise shift from mixed to structured representations. Furthermore, simple steering—shifting along centroid-based directions between topic subspaces—induces causal and interpretable changes in model behavior (e.g., step-by-step reasoning without CoT prompting), suggesting that CoT behavior can be encoded in a single vector matching the model’s hidden dimensionality.

These findings provide compelling evidence that transformer-based LLMs develop an internal geometry that is both semantically structured and computationally efficient. This perspective opens avenues for building alignment tools and control mechanisms that operate directly in latent space—for example, the MLP we train on a single layer achieves high precision in distinguishing benign from malicious prompts, regardless of narrative—enabling targeted interventions without modifying model weights or relying on external supervision.

References

- [1] Armen Aghajanyan, Sonal Gupta, and Luke Zettlemoyer. Intrinsic dimensionality explains the effectiveness of language model fine-tuning. In Chengqing Zong, Fei Xia, Wenjie Li, and Roberto Navigli, editors, *Proceedings of the 59th Annual Meeting of the Association for Computational Linguistics and the 11th International Joint Conference on Natural Language Processing (Volume 1: Long Papers)*, pages 7319–7328, Online, August 2021. Association for Computational Linguistics. doi: 10.18653/v1/2021.acl-long.568. URL <https://aclanthology.org/2021.acl-long.568/>.
- [2] Mistral AI. Mistral small. <https://huggingface.co/mistralai/Mistral-Small>, 2024. Accessed: 2025-03-17.
- [3] AI@Meta. Llama 3 model card. 2024. URL https://github.com/meta-llama/llama3/blob/main/MODEL_CARD.md.

[4] Alessio Ansuini, Alessandro Laio, Jakob H Macke, and Davide Zoccolan. Intrinsic dimension of data representations in deep neural networks. In H. Wallach, H. Larochelle, A. Beygelzimer, F. d'Alché-Buc, E. Fox, and R. Garnett, editors, *Advances in Neural Information Processing Systems*, volume 32. Curran Associates, Inc., 2019. URL https://proceedings.neurips.cc/paper_files/paper/2019/file/cfcce0621b49c983991ead4c3d4d3b6b-Paper.pdf.

[5] Amos Azaria and Tom Mitchell. The internal state of an LLM knows when it's lying. In *The 2023 Conference on Empirical Methods in Natural Language Processing*, 2023. URL <https://openreview.net/forum?id=y2V6YgLaW7>.

[6] Daniel Beaglehole, Adityanarayanan Radhakrishnan, Enric Boix-Adserà, and Mikhail Belkin. Aggregate and conquer: detecting and steering llm concepts by combining nonlinear predictors over multiple layers, 2025. URL <https://arxiv.org/abs/2502.03708>.

[7] Yonatan Belinkov, Nadir Durrani, Fahim Dalvi, Hassan Sajjad, and James Glass. What do neural machine translation models learn about morphology? In Regina Barzilay and Min-Yen Kan, editors, *Proceedings of the 55th Annual Meeting of the Association for Computational Linguistics (Volume 1: Long Papers)*, pages 861–872, Vancouver, Canada, July 2017. Association for Computational Linguistics. doi: 10.18653/v1/P17-1080. URL <https://aclanthology.org/P17-1080/>.

[8] Nicolas Bonneel, Julien Rabin, Gabriel Peyré, and Hanspeter Pfister. Sliced and radon wasserstein barycenters of measures. *J. Math. Imaging Vis.*, 51(1):22–45, January 2015.

[9] Tom B. Brown, Benjamin Mann, Nick Ryder, Melanie Subbiah, Jared Kaplan, Prafulla Dhariwal, Arvind Neelakantan, Pranav Shyam, Girish Sastry, Amanda Askell, Sandhini Agarwal, Ariel Herbert-Voss, Gretchen Krueger, Tom Henighan, Rewon Child, Aditya Ramesh, Daniel M. Ziegler, Jeffrey Wu, Clemens Winter, Christopher Hesse, Mark Chen, Eric Sigler, Mateusz Litwin, Scott Gray, Benjamin Chess, Jack Clark, Christopher Berner, Sam McCandlish, Alec Radford, Ilya Sutskever, and Dario Amodei. Language models are few-shot learners, 2020.

[10] Collin Burns, Haotian Ye, Dan Klein, and Jacob Steinhardt. Discovering latent knowledge in language models without supervision, 2024. URL <https://arxiv.org/abs/2212.03827>.

[11] Xingyu Cai, Jiaji Huang, Yuchen Bian, and Kenneth Church. Isotropy in the contextual embedding space: Clusters and manifolds. In *International Conference on Learning Representations*, 2021. URL <https://openreview.net/forum?id=xYGN0860WDH>.

[12] Colin B. Clement, Matthew Bierbaum, Kevin P. O’Keeffe, and Alexander A. Alemi. On the use of arxiv as a dataset, 2019. URL <https://arxiv.org/abs/1905.00075>.

[13] Karl Cobbe, Vineet Kosaraju, Mohammad Bavarian, Mark Chen, Heewoo Jun, Lukasz Kaiser, Matthias Plappert, Jerry Tworek, Jacob Hilton, Reiichiro Nakano, Christopher Hesse, and John Schulman. Training verifiers to solve math word problems. *arXiv preprint arXiv:2110.14168*, 2021.

[14] Alexis Conneau, German Kruszewski, Guillaume Lample, Loïc Barrau, and Marco Baroni. What you can cram into a single \$&#!#* vector: Probing sentence embeddings for linguistic properties. In Iryna Gurevych and Yusuke Miyao, editors, *Proceedings of the 56th Annual Meeting of the Association for Computational Linguistics (Volume 1: Long Papers)*, pages 2126–2136, Melbourne, Australia, July 2018. Association for Computational Linguistics. doi: 10.18653/v1/P18-1198. URL <https://aclanthology.org/P18-1198/>.

[15] Sumanth Dathathri, Andrea Madotto, Janice Lan, Jane Hung, Eric Frank, Piero Molino, Jason Yosinski, and Rosanne Liu. Plug and play language models: A simple approach to controlled text generation. In *International Conference on Learning Representations*, 2020. URL <https://openreview.net/forum?id=H1edEyBKDS>.

[16] Nelson Elhage, Tristan Hume, Catherine Olsson, Nicholas Schiefer, Tom Henighan, Shauna Kravec, Zac Hatfield-Dodds, Robert Lasenby, Dawn Drain, Carol Chen, Roger Grosse, Sam McCandlish, Jared Kaplan, Dario Amodei, Martin Wattenberg, and Christopher Olah. Toy models of superposition, 2022. URL <https://arxiv.org/abs/2209.10652>.

[17] Joshua Engels, Eric J Michaud, Isaac Liao, Wes Gurnee, and Max Tegmark. Not all language model features are one-dimensionally linear. In *The Thirteenth International Conference on Learning Representations*, 2025. URL <https://openreview.net/forum?id=d63a4AM4hb>.

[18] Kawin Ethayarajh. How contextual are contextualized word representations? Comparing the geometry of BERT, ELMo, and GPT-2 embeddings. In Kentaro Inui, Jing Jiang, Vincent Ng, and Xiaojun Wan, editors, *Proceedings of the 2019 Conference on Empirical Methods in Natural Language Processing and the 9th International Joint Conference on Natural Language Processing (EMNLP-IJCNLP)*, pages 55–65, Hong Kong, China, November 2019. Association for Computational Linguistics. doi: 10.18653/v1/D19-1006. URL <https://aclanthology.org/D19-1006/>.

[19] Jun Gao, Di He, Xu Tan, Tao Qin, Liwei Wang, and Tieyan Liu. Representation degeneration problem in training natural language generation models. In *International Conference on Learning Representations*, 2019. URL <https://openreview.net/forum?id=SkEYojRqtm>.

[20] Nathan Godey, Éric Clergerie, and Benoît Sagot. Anisotropy is inherent to self-attention in transformers. In Yvette Graham and Matthew Purver, editors, *Proceedings of the 18th Conference of the European Chapter of the Association for Computational Linguistics (Volume 1: Long Papers)*, pages 35–48, St. Julian’s, Malta, March 2024. Association for Computational Linguistics. URL <https://aclanthology.org/2024.eacl-long.3/>.

[21] Sylvain Gugger, Lysandre Debut, Thomas Wolf, Philipp Schmid, Zachary Mueller, Sourab Mangrulkar, Marc Sun, and Benjamin Bossan. Accelerate: Training and inference at scale made simple, efficient and adaptable. <https://github.com/huggingface/accelerate>, 2022.

[22] Michael Hanna, Yonatan Belinkov, and Sandro Pezzelle. Are formal and functional linguistic mechanisms dissociated in language models?, 2025. URL <https://arxiv.org/abs/2503.11302>.

[23] Dan Hendrycks, Collin Burns, Steven Basart, Andy Zou, Mantas Mazeika, Dawn Song, and Jacob Steinhardt. Measuring massive multitask language understanding. *Proceedings of the International Conference on Learning Representations (ICLR)*, 2021.

[24] John Hewitt and Christopher D. Manning. A structural probe for finding syntax in word representations. In Jill Burstein, Christy Doran, and Thamar Solorio, editors, *Proceedings of the 2019 Conference of the North American Chapter of the Association for Computational Linguistics: Human Language Technologies, Volume 1 (Long and Short Papers)*, pages 4129–4138, Minneapolis, Minnesota, June 2019. Association for Computational Linguistics. doi: 10.18653/v1/N19-1419. URL <https://aclanthology.org/N19-1419/>.

[25] Albert Q. Jiang, Alexandre Sablayrolles, Arthur Mensch, Chris Bamford, Devendra Singh Chaplot, Diego de las Casas, Florian Bressand, Gianna Lengyel, Guillaume Lample, Lucile Saulnier, Lélio Renard Lavaud, Marie-Anne Lachaux, Pierre Stock, Teven Le Scao, Thibaut Lavril, Thomas Wang, Timothée Lacroix, and William El Sayed. Mistral 7b, 2023. URL <https://arxiv.org/abs/2310.06825>.

[26] Albert Q. Jiang, Alexandre Sablayrolles, Antoine Roux, Arthur Mensch, Blanche Savary, Chris Bamford, Devendra Singh Chaplot, Diego de las Casas, Emma Bou Hanna, Florian Bressand, Gianna Lengyel, Guillaume Bour, Guillaume Lample, Lélio Renard Lavaud, Lucile Saulnier, Marie-Anne Lachaux, Pierre Stock, Sandeep Subramanian, Sophia Yang, Szymon Antoniak, Teven Le Scao, Théophile Gervet, Thibaut Lavril, Thomas Wang, Timothée Lacroix, and William El Sayed. Mixtral of experts, 2024. URL <https://arxiv.org/abs/2401.04088>.

[27] Liwei Jiang, Kavel Rao, Seungju Han, Allyson Ettinger, Faeze Brahman, Sachin Kumar, Niloofar Mireshghallah, Ximing Lu, Maarten Sap, Yejin Choi, and Nouha Dziri. Wildteam-ing at scale: From in-the-wild jailbreaks to (adversarially) safer language models. In *The Thirty-eighth Annual Conference on Neural Information Processing Systems*, 2024. URL <https://openreview.net/forum?id=n5R6TvBVcX>.

[28] Riku Kisako, Tatsuki Kuribayashi, and Ryohei Sasano. On representational dissociation of language and arithmetic in large language models, 2025. URL <https://arxiv.org/abs/2502.11932>.

[29] Nelson F. Liu, Matt Gardner, Yonatan Belinkov, Matthew E. Peters, and Noah A. Smith. Linguistic knowledge and transferability of contextual representations. In Jill Burstein, Christy Doran, and Thamar Solorio, editors, *Proceedings of the 2019 Conference of the North American Chapter of the Association for Computational Linguistics: Human Language Technologies, Volume 1 (Long and Short Papers)*, pages 1073–1094, Minneapolis, Minnesota, June 2019. Association for Computational Linguistics. doi: 10.18653/v1/N19-1112. URL <https://aclanthology.org/N19-1112/>.

[30] Kyle Mahowald, Anna A. Ivanova, Idan A. Blank, Nancy Kanwisher, Joshua B. Tenenbaum, and Evelina Fedorenko. Dissociating language and thought in large language models. *Trends in Cognitive Sciences*, 28(6):517–540, 2024. ISSN 1364-6613. doi: <https://doi.org/10.1016/j.tics.2024.01.011>. URL <https://www.sciencedirect.com/science/article/pii/S1364661324000275>.

[31] Samuel Marks and Max Tegmark. The geometry of truth: Emergent linear structure in large language model representations of true/false datasets. In *First Conference on Language Modeling*, 2024. URL <https://openreview.net/forum?id=aaajyHYjjsk>.

[32] Edi Muskardin, Martin Tappler, Ingo Pill, Bernhard Aichernig, and Thomas Pock. On the relationship between RNN hidden-state vectors and semantic structures. In Lun-Wei Ku, Andre Martins, and Vivek Srikumar, editors, *Findings of the Association for Computational Linguistics: ACL 2024*, pages 5641–5658, Bangkok, Thailand, August 2024. Association for Computational Linguistics. doi: 10.18653/v1/2024.findings-acl.335. URL <https://aclanthology.org/2024.findings-acl.335/>.

[33] Neel Nanda, Andrew Lee, and Martin Wattenberg. Emergent linear representations in world models of self-supervised sequence models. In Yonatan Belinkov, Sophie Hao, Jaap Jumelet, Najoung Kim, Arya McCarthy, and Hosein Mohebbi, editors, *Proceedings of the 6th BlackboxNLP*

Workshop: Analyzing and Interpreting Neural Networks for NLP, pages 16–30, Singapore, December 2023. Association for Computational Linguistics. doi: 10.18653/v1/2023.blackboxnlp-1.2. URL <https://aclanthology.org/2023.blackboxnlp-1.2/>.

- [34] Hadas Orgad, Michael Toker, Zorik Gekhman, Roi Reichart, Idan Szpektor, Hadas Kotek, and Yonatan Belinkov. LLMs know more than they show: On the intrinsic representation of LLM hallucinations. In *The Thirteenth International Conference on Learning Representations*, 2025. URL <https://openreview.net/forum?id=KRnsX5Em3W>.
- [35] Kiho Park, Yo Joong Choe, and Victor Veitch. The linear representation hypothesis and the geometry of large language models. In *Proceedings of the 41st International Conference on Machine Learning*, ICML'24. JMLR.org, 2024.
- [36] Alec Radford, Jeff Wu, Rewon Child, David Luan, Dario Amodei, and Ilya Sutskever. Language models are unsupervised multitask learners. 2019.
- [37] Sebastian Raschka, Joshua Patterson, and Corey Nolet. Machine learning in python: Main developments and technology trends in data science, machine learning, and artificial intelligence. *Information (Basel)*, 11(4):193, April 2020.
- [38] Anton Razzhigaev, Matvey Mikhalkuk, Elizaveta Goncharova, Ivan Oseledets, Denis Dimitrov, and Andrey Kuznetsov. The shape of learning: Anisotropy and intrinsic dimensions in transformer-based models. In Yvette Graham and Matthew Purver, editors, *Findings of the Association for Computational Linguistics: EACL 2024*, pages 868–874, St. Julian’s, Malta, March 2024. Association for Computational Linguistics. URL <https://aclanthology.org/2024.findings-eacl.58/>.
- [39] Paul Röttger, Hannah Kirk, Bertie Vidgen, Giuseppe Attanasio, Federico Bianchi, and Dirk Hovy. XSTest: A test suite for identifying exaggerated safety behaviours in large language models. In Kevin Duh, Helena Gomez, and Steven Bethard, editors, *Proceedings of the 2024 Conference of the North American Chapter of the Association for Computational Linguistics: Human Language Technologies (Volume 1: Long Papers)*, pages 5377–5400, Mexico City, Mexico, June 2024. Association for Computational Linguistics. doi: 10.18653/v1/2024.naacl-long.301. URL <https://aclanthology.org/2024.naacl-long.301/>.
- [40] Baturay Saglam, Zhuoran Yang, Dionysis Kalogerias, and Amin Karbasi. Learning task representations from in-context learning, 2025. URL <https://arxiv.org/abs/2502.05390>.
- [41] Oscar Skean, Md Rifat Arefin, Dan Zhao, Niket Patel, Jalal Naghiyev, Yann LeCun, and Ravid Shwartz-Ziv. Layer by layer: Uncovering hidden representations in language models, 2025. URL <https://arxiv.org/abs/2502.02013>.
- [42] Jianlin Su, Yu Lu, Shengfeng Pan, Ahmed Murtadha, Bo Wen, and Yunfeng Liu. Roformer: Enhanced transformer with rotary position embedding, 2023. URL <https://arxiv.org/abs/2104.09864>.
- [43] Alon Talmor, Jonathan Herzig, Nicholas Lourie, and Jonathan Berant. CommonsenseQA: A question answering challenge targeting commonsense knowledge. In Jill Burstein, Christy Doran, and Thamar Solorio, editors, *Proceedings of the 2019 Conference of the North American Chapter of the Association for Computational Linguistics: Human Language Technologies, Volume 1 (Long and Short Papers)*, pages 4149–4158, Minneapolis, Minnesota, June 2019. Association for

Computational Linguistics. doi: 10.18653/v1/N19-1421. URL <https://aclanthology.org/N19-1421/>.

- [44] Rachel Tatman. English word frequency. Kaggle dataset, 2020. <https://www.kaggle.com/datasets/rtatman/english-word-frequency>.
- [45] Gemma Team. Gemma 2: Improving open language models at a practical size, 2024. URL <https://arxiv.org/abs/2408.00118>.
- [46] Ian Tenney, Dipanjan Das, and Ellie Pavlick. BERT rediscovers the classical NLP pipeline. In Anna Korhonen, David Traum, and Lluís Màrquez, editors, *Proceedings of the 57th Annual Meeting of the Association for Computational Linguistics*, pages 4593–4601, Florence, Italy, July 2019. Association for Computational Linguistics. doi: 10.18653/v1/P19-1452. URL <https://aclanthology.org/P19-1452/>.
- [47] Lucrezia Valeriani, Diego Doimo, Francesca Cuturello, Alessandro Laio, Alessio ansuini, and Alberto Cazzaniga. The geometry of hidden representations of large transformer models. In *Thirty-seventh Conference on Neural Information Processing Systems*, 2023. URL <https://openreview.net/forum?id=cCYvakU5Ek>.
- [48] Ashish Vaswani, Noam Shazeer, Niki Parmar, Jakob Uszkoreit, Llion Jones, Aidan N Gomez, Łukasz Kaiser, and Illia Polosukhin. Attention is all you need. In I. Guyon, U. Von Luxburg, S. Bengio, H. Wallach, R. Fergus, S. Vishwanathan, and R. Garnett, editors, *Advances in Neural Information Processing Systems*, volume 30. Curran Associates, Inc., 2017. URL https://proceedings.neurips.cc/paper_files/paper/2017/file/3f5ee243547dee91fdb053c1c4a845aa-Paper.pdf.
- [49] Laura Weidinger, Jonathan Uesato, Maribeth Rauh, Conor Griffin, Po-Sen Huang, John Mellor, Amelia Glaese, Myra Cheng, Borja Balle, Atoosa Kasirzadeh, Courtney Biles, Sasha Brown, Zac Kenton, Will Hawkins, Tom Stepleton, Abeba Birhane, Lisa Anne Hendricks, Laura Rimell, William Isaac, Julia Haas, Sean Legassick, Geoffrey Irving, and Iason Gabriel. Taxonomy of risks posed by language models. In *Proceedings of the 2022 ACM Conference on Fairness, Accountability, and Transparency*, FAccT '22, page 214–229, New York, NY, USA, 2022. Association for Computing Machinery. ISBN 9781450393522. doi: 10.1145/3531146.3533088. URL <https://doi.org/10.1145/3531146.3533088>.
- [50] Thomas Wolf, Lysandre Debut, Victor Sanh, Julien Chaumond, Clement Delangue, Anthony Moi, Pierrick Cistac, Tim Rault, Rémi Louf, Morgan Funtowicz, Joe Davison, Sam Shleifer, Patrick von Platen, Clara Ma, Yacine Jernite, Julien Plu, Canwen Xu, Teven Le Scao, Sylvain Gugger, Mariama Drame, Quentin Lhoest, and Alexander M. Rush. Transformers: State-of-the-art natural language processing. In *Proceedings of the 2020 Conference on Empirical Methods in Natural Language Processing: System Demonstrations*, pages 38–45, Online, October 2020. Association for Computational Linguistics. URL <https://www.aclweb.org/anthology/2020.emnlp-demos.6>.
- [51] Zhenhong Zhou, Haiyang Yu, Xinghua Zhang, Rongwu Xu, Fei Huang, Kun Wang, Yang Liu, Junfeng Fang, and Yongbin Li. On the role of attention heads in large language model safety. In *The Thirteenth International Conference on Learning Representations*, 2025. URL <https://openreview.net/forum?id=h0Ak8A5yqw>.

A Experimental Details

A.1 Datasets

Detailed statistics—covering the number of samples and token-level properties (minimum, maximum, mean, and median)—are provided in Table 7.

A.1.1 arXiv Abstracts

The arXiv metadata dataset [12], curated by researchers at Cornell University, contains metadata for 1.7 million articles submitted to arXiv over the past 30 years. This metadata includes fields such as article titles, authors, categories, and abstracts. To ensure consistency in length and structure across domains, we used only the abstracts as the source text for the topics. The arXiv taxonomy and subtopics are detailed in their website².

A.1.2 Chain-of-Thought

CommonsenseQA [43] A multiple-choice question (MCQ) dataset that requires various types of commonsense knowledge to predict the correct answer.

Dataset	# Samples	# Tokens			
		Max	Min	Mean	Median
Computer Science (CS)	20,000	630	20	235.96	234
Electrical Engineering and System Science (EESS)	14,560	599	20	237.56	235
Math	20,000	783	20	161.15	141
Physics	20,000	752	20	219.35	204
Biology	16,764	983	20	246.48	245
Statistics	20,000	993	20	221.37	221
CommonsenseQA	10,962	102	29	44.59	43
GSM8K	8,792	215	17	63.56	60
MMLU	14,275	235	25	82.70	70
Vanilla benign	50,050	41	6	15.99	15
Vanilla harmful	50,050	69	6	20.38	19
Adversarial benign	78,731	39	6	15.89	15
Adversarial harmful	82,728	69	6	20.32	19

* Abstracts with fewer than 20 tokens were discarded.

Table 7: Number of samples and final token-level statistics for each dataset. For abstract-based datasets, we cap each sample at 750 tokens and limit the total number of samples to 20,000. No preprocessing—other than basic string operations such as whitespace stripping—was applied.

GSM8K [13] A dataset of high-quality, linguistically diverse grade school math word problems designed to support question answering tasks that require multi-step reasoning.

MMLU [23] An MCQ dataset covering a broad range of subjects in the humanities, social sciences, hard sciences, and other fields. It spans 57 tasks, including elementary mathematics, U.S. history, computer science, and law. Achieving high accuracy on MMLU requires extensive world knowledge and strong problem-solving ability.

A.1.3 Alignment – WildJailbreak [27]

Vanilla Harmful Direct requests that could elicit harmful responses from LMs. Jiang et al. [27] used GPT-4 to synthetically generate 50,500 vanilla harmful prompts across 13 risk categories, based on the taxonomy from Weidinger et al. [49]. Each prompt is paired with a helpful, detailed refusal response generated by GPT-3.5 [9].

Vanilla Benign Harmless prompts designed to address exaggerated safety behaviors (i.e., over-refusal on benign queries). Using categories from XSTest [39], GPT-4 generates 50,050 prompts that superficially resemble unsafe prompts by keywords or sensitive topics but remain non-harmful. Complying responses are generated with GPT-3.5.

Adversarial Harmful Adversarial jailbreaks embedding harmful requests in more convoluted and stealthy forms. Authors’ proposed WildTeaming framework was applied to transform vanilla harmful queries using 2–7 randomly sampled In-the-Wild jailbreak tactics, employing Mixtral-8×7B [26] and GPT-4. After filtering out low-risk and off-topic prompts, adversarial prompts are paired with the refusal responses of their vanilla counterparts, resulting in 82,728 items.

Adversarial Benign Adversarial queries that appear as jailbreaks but carry no harmful intent. Jiang et al. [27] created 78,706 such prompts using WildTeaming based on vanilla benign queries, with GPT-3.5 used to generate direct, compliant continuations.

A.2 Implementation

Computing Infrastructure All experiments were conducted using the infrastructure provided by Crusoe AI³. Hidden states were collected using two nodes in parallel, each equipped with 8×80 GB H100 GPUs.

Models and Collecting Hidden States All models used in this study are open-source and accessed via Hugging Face using the transformers library [50]. We used accelerate [21] to distribute inference across 8 GPUs.

Fitting SVM for Linear Separability We used the cuML library [37] for its efficient GPU-accelerated SVM implementation. While standard SVMs minimize $\frac{1}{2}\|\mathbf{w}\|^2$ as in (1), one could instead solve for any separating \mathbf{w} without regularization—but no CUDA-supported implementation exists for such unregularized methods. cuML, part of NVIDIA’s RAPIDS suite, runs training entirely on GPU using parallelized updates and matrix operations. We ran the SVM for 10^9 iterations per topic pair, completing each test in under a minute. In contrast, CPU-based solvers and GPU-based gradient descent took over 10 minutes per pair, largely due to the high dimensionality. With thousands of separability tests, cuML provides a practical and scalable solution for our large-scale analysis.

³<https://crusoe.ai>

Answer the following question. Think step by step and show all your reasoning before giving the final answer.

Where could there be a cloud?

- A) Air
- B) Night or day
- C) Weather report
- D) Atmosphere
- E) Above rain

Figure 5: An example question from CommonsenseQA with the chain-of-thought instruction.

Wasserstein Distance While the Wasserstein metric is conceptually powerful, it is computationally intensive. Optimizations such as Sinkhorn regularization or random projections are commonly used to reduce complexity. In our setting, however—due to the high dimensionality and large number of samples—even the Sinkhorn approximation proved computationally infeasible. We therefore used the sliced Wasserstein distance [8], computed with 3000 random projections.

Formatting Chain-of-Thought Prompts Each question from CommonsenseQA, GSM8K, and MMLU is initially formatted with a standard instruction: “Answer the following question.” For the CoT variant, we append the instruction “Think step by step and show all your reasoning before giving the final answer.” immediately after this sentence. An example prompt is provided in Figure 5.

B Supplementary Results

B.1 Example Texts Under Varying Masking Thresholds

In Figures 6, 7, and 8, we show an example abstract from computer science (machine learning, “cs.LG”) and its 10% and 50% masked versions, respectively. With only 10% masking, the abstract remains nearly intact—the loss of a single technical term (“Markovity”) has minimal impact on global semantics, so a linear probe would still classify its representation within the computer science cluster. After 50% masking, however, many diagnostic nouns (e.g., “replay buffer,” “reinforcement,” “convergence”) and function words are removed, yielding a syntactically degraded but still coherent scaffold. This heavier masking weakens lexical signals, forcing the classifier to rely on higher-level features such as clause structure, residual technical collocations (e.g., “stochastic process,” “analysis”), and the rhetorical form of the abstract. The comparison illustrates how domain identity can persist through substantial lexical ablation, but becomes increasingly dependent on distributed, non-keyword cues as masking intensifies.

B.2 Supplementary Validation of Linearity via Simple Steering

Another convenient and interpretable way to test the linearity is to steer the model by adding the vector

$$\Delta_\mu = \mu_{t_2} - \mu_{t_1} = \frac{1}{N_{t_2}} \sum_{i=1}^{N_{t_2}} \mathbf{X}_i^{(t_2)} - \frac{1}{N_{t_1}} \sum_{i=1}^{N_{t_1}} \mathbf{X}_i^{(t_1)},$$

Replay buffers are a key component in many reinforcement learning schemes. Yet, their theoretical properties are not fully understood. In this paper we analyze a system where a stochastic process X is pushed into a replay buffer and then randomly sampled to generate a stochastic process Y from the replay buffer. We provide an analysis of the properties of the sampled process such as stationarity, Markovity and autocorrelation in terms of the properties of the original process. Our theoretical analysis sheds light on why replay buffer may be a good de-correlator. Our analysis provides theoretical tools for proving the convergence of replay buffer based algorithms which are prevalent in reinforcement learning schemes.

Figure 6: An example abstract from *computer science* (machine learning, “cs.LG”).

Replay buffers are a key component in many reinforcement learning schemes. Yet, their theoretical properties are not fully understood. In this paper we analyze a system where a stochastic process X is pushed into a replay buffer and then randomly sampled to generate a stochastic process Y from the replaybuffer. We provide an analysis of the properties of the sampled process such as stationarity, autocorrelation and autocorrelation in terms of the properties of the original process. Our theoretical analysis sheds light on why replay buffer may be a good de-correlator. Our analysis provides theoretical tools for proving the convergence of replay buffer based algorithms which are prevalent in reinforcement learning schemes.

Figure 7: The same abstract shown in Figure 6, masked using a 10% frequency threshold. The text remains semantically meaningful, and it is still easy to infer that it comes from a machine learning article.

for steering from topic t_1 to t_2 . This vector is then added to the hidden state at the final token position of a selected layer L :

$$\tilde{\mathbf{h}}^{(L)} \leftarrow \mathbf{h}^{(L)} + \alpha \cdot \mathbf{v}_{t_1 \rightarrow t_2},$$

where $\mathbf{h}^{(L)} \in \mathbb{R}^d$ is the original hidden state, $\alpha \in \mathbb{R}$ is a scalar controlling the intervention strength, and $\tilde{\mathbf{h}}^{(L)}$ is the modified hidden state used for subsequent computation.

Because Δ_μ is the normal of the maximal-margin hyperplane that separates the clusters, it is the most information-efficient direction for altering membership: translating an activation along Δ_μ moves it toward the target subspace while minimally disturbing orthogonal features. The construction is fully unsupervised (no gradient updates or auxiliary labels are required), architecture-agnostic, and parameter-free apart from a scalar step size, ensuring that any observed change in output can be attributed directly to the identified linear dimension. Demonstrating that small perturbations of magnitude $\alpha\Delta_\mu$ induce monotonic shifts in generation therefore provides a causal, geometry-consistent validation of the hypothesis that high-level semantics are encoded additively along low-dimensional directions.

We sampled 100 random questions from the selected benchmark datasets and had models respond with and without steering, setting α to match the norm of the original hidden state. Manual inspection of the outputs reveals intuitive patterns: models with more structured hidden state clusters—such as Mistral-24B compared to Llama 3.1-8B—exhibit CoT behavior more frequently.

----- are a key component in many ----- learning -----.
Yet, their ----- properties are not fully -----.
In this paper we ----- a system where a ----- process X is ----- into a -----
and then ----- to generate a ----- process Y from the -----
----- We provide an analysis of the properties of the -----
process such as -----, ----- and ----- in terms of the
properties of the original process. Our ----- analysis ----- light on
why ----- may be a good de-----.
Our analysis provides ----- tools for ----- the ----- of ----- based
----- which are ----- in ----- learning -----.

Figure 8: The same abstract shown in Figure 6, masked using a 50% frequency threshold. While it remains identifiable as technical—possibly from an engineering-related field—it becomes clearly impossible to determine the exact topic (e.g., electrical engineering, computer science, or statistics).

Representative outputs under non-CoT, CoT, and steered prompts are shown in Figures 9 and 10. Notably, Mistral-24B produces more coherent shifts than Llama 3.1-8B, as evidenced by clearer CoT markers like “step by step.” However, increasing the steering scalar α beyond a certain threshold distorts the hidden states and results in gibberish outputs, limiting the effective steering range.

This suggests that linear separability is not merely a diagnostic of semantic organization, but also a practical tool for causal intervention—reinforcing the view that well-structured latent spaces enable more controllable generation. Furthermore, these results indicate that CoT reasoning can be encoded into a single vector of model dimensionality. That said, further validation with larger sample sizes and automated methods for assessing reasoning quality is likely needed, which we leave for future work.

<p>A) Wrong, Not wrong</p> <p>In Scenario 1, taking food from a clearly starving dog...</p> <p>In Scenario 2, bringing the mother-in-law to see "Titanic"...</p>	<p>To determine which scenario is morally wrong, let's analyze each one step by step according to ordinary moral standards in the US as of 2020.</p> <p>Scenario 1:...</p> <p>Scenario 2:...</p> <p>Therefore, the correct answer is:</p> <p>A) Wrong, Not wrong</p>	<p>Let's analyze each scenario according to ordinary moral standards in the US as of 2020:</p> <p>Scenario 1:...</p> <p>Scenario 2:...</p> <p>Therefore, the correct answer is: A) Wrong, Not wrong</p>
<p>(a) Non-CoT Output</p>	<p>(b) CoT Output</p>	<p>(c) Steering: Non-CoT → CoT</p>

Figure 9: Comparison of Llama 3.1-8B outputs for an MMLU question: “For which of these two scenarios does the main character (who uses I/me/my) do something clearly morally wrong, according to ordinary moral standards in the US as of 2020? Scenario 1 | I took the food from the clearly starving dog. Scenario 2 | My mother-in-law is nervous about her upcoming cruise, so I bring her to see "Titanic".” with four choices. Responses were generated using deterministic sampling (temperature = 0.0). Steering was applied at the final layer.

<p>The correct answer is D) Venice. Venice, Italy, is famous for its extensive network of canals, which are a defining feature of the city. The city is built on an archipelago of 118 small islands connected by bridges, and its canals serve as the main transportation routes.</p>	<p>To determine where in Southern Europe you would find many canals, let's reason through the options step by step:</p> <ol style="list-style-type: none"> **Michigan**: This is a state in the United States, not in Southern Europe. **Venice**: Venice is a city in Italy, which is in Southern Europe. : **Amsterdam**: <p>Given this reasoning, the correct answer is:</p> <p>D) Venice</p>	<p>To determine where in Southern Europe we would find many canals, let's analyze the options step by step:</p> <ol style="list-style-type: none"> **Michigan**: This is a state in the United States, not in Southern Europe. **Venice**: Venice is in Italy, which is in Southern Europe. Venice is famous for its canals. : **Amsterdam**: <p>Therefore, the correct answer is:</p> <p>D) Venice</p>
<p>(a) Non-CoT Output</p>	<p>(b) CoT Output</p>	<p>(c) Steering: Non-CoT → CoT</p>

Figure 10: Comparison of Mistral-24B outputs for a CommonsenseQA question: “Where in Southern Europe would you find many canals?” with five city options provided as answer choices. Responses were generated using deterministic sampling (temperature = 0.0). Steering was applied at the final layer.